High-Order Wavelet Reconstruction for Multi-Scale Edge Aware Tone Mapping

Alessandro Artusi[a], Zhuo Su[b,c], Zongwei Zhang's[b,c], Dimitris Drikakis[d], Xiaonan Luo[b,c]

[a]*Graphics and Imaging Laboratory Department of Informatics and Applied Mathematics University of Girona.*
[b]*National Engineering Research Center of Digital Life, Guangzhou, China.*
[c]*School of Information Science and Technology, Sun Yat-sen University, Guangzhou, China.*
[d]*Fluid Mechanics and Computational Science Cranfield University.*

Abstract

This paper presents a High Order Reconstruction (HOR) method for improved multi-scale edge aware tone mapping. The study aims to contribute to the improvement of edge-aware techniques for smoothing an input image, while keeping its edges intact. The proposed HOR methods circumvent limitations of the existing state of the art methods, e.g., altering the image structure due to changes in contrast; remove artefacts around edges; as well as reducing computational complexity in terms of implementation and associated computational costs. In particular, the proposed method aims at reducing the changes in the image structure by intrinsically enclosing an edge-stop mechanism whose computational cost is comparable to the state-of-the-art multi-scale edge aware techniques.

Keywords:

1. Introduction

High Order Reconstruction (HOR) methods, introduced by Harten et al. [1], have been used extensively for solving the hyperbolic conservation laws and the Hamilton-Jacobi equations [2]. Additionally, these methods have been applied to image processing (image compression), denoising [3] and segmentation [4]. Due to their ability to reduce oscillations around function discontinuities, these methods can be potentially used as an edge aware interpolation tool. Edge-aware techniques such as anisotropic diffusion [5], bilateral filtering [6, 7] and neighborhood filtering rely on sophisticated type of spatially varying kernels. Often, they tend to either generate artificially staircasing effects or ringing effects around sharp edges [8]. These artifacts can be reduced using a post-processing step at the price of increasing the computational cost and the number of parameters used [9]. To have better control of the details over the spatial scale, one can apply edge-aware techniques in a multi-scale fashion. However, the bilateral filtering is inappropriate for multi-scale detailed decomposition [10]. Other edge-aware techniques that support the multi-scale approach [10, 11, 9] also encompass some flaws, e.g., they are not able to achieve a plausible reproduction of all important image features [12] and may change the image structure.
Therefore, there is a need to develop methods that are reducing as much as possible any change into the image structure without increasing the complexity or computational cost.

In this paper, we link the edge-aware problem to the typical problem of interpolation. In particular, we propose a novel wavelet scheme that uses a robust predictor operator, based on the HOR method, which intrinsically encloses an edge-stop mechanism to avoid influence of pixels from both sides of an edge. To have a better control of details over the spatial scale, we employ the HOR method in conjunction with a multi-scale scheme.
We demonstrate the usability of the proposed method to solve a typical problem in the context of High Dynamic Range (HDR) imaging, called tone mapping as defined in Banterle et al. [13].

The approach is formulated as follows; we decompose an input HDR image, making use of wavelet decomposition and through the use of HOR methods separate its coarse and fine features (details). The coarse and fine features are then manipulated to achieve the desired tone and details levels. Finally, the output image is reconstructed. The advantage of the above approach is that it does not require the introduction of any edge-stopping function that limits possible image-structure changes.

To understand this concept, Figure 1 shows the distortion map as output of the Dynamic Range Indepen-

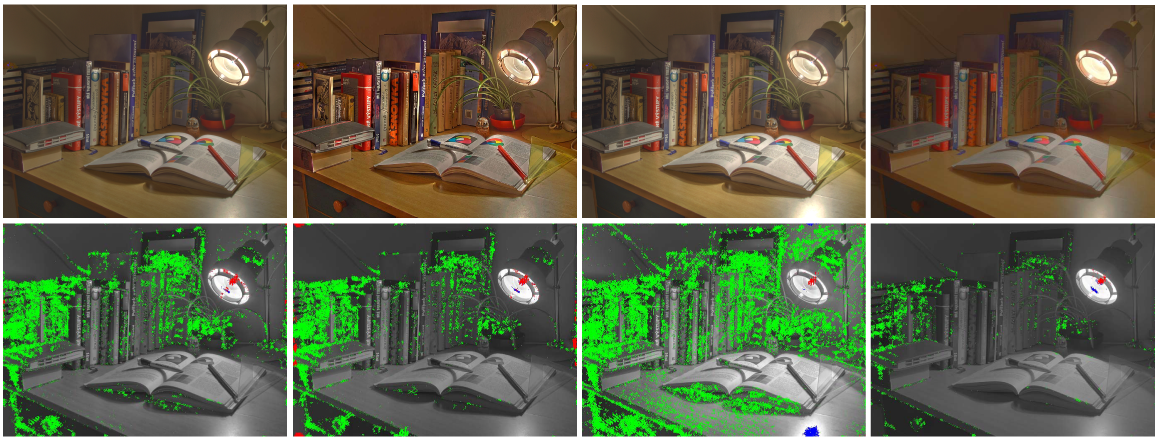

Figure 1: Comparison of the state-of-the-art multiscale edge aware based tone mapping operators and the present HOR: 1st row: output of the various techniques. 2nd row: distortion map of the DRIM metric [12]. This map is showing the pixels that shows a distorsion with 95% of probability to been seen by the Human Visual System (HVS). Blue pixels are areas where invisible contrast is introduced; red pixels are areas where reversal of visible contrast is noticeable and green pixels shows areas of lost of contrast. The map is showing of a reduction of more than 50% of the pixels affected by loss of contrast when the the HOR method is used. Parameters used - Farbmann et al. [10] multiscale approach balanced - Fattal's [11] $\alpha = 0.9$, $\beta = 0.16$ and $\gamma = 0.8$ - Paris et al. [9] $\sigma_r = log(2.5)$, $\alpha = 0.5$ and $\beta = 0.0$ (for conveying the local effect) - The Present HOR $\beta = 0.7$, $\gamma = 0.9$.

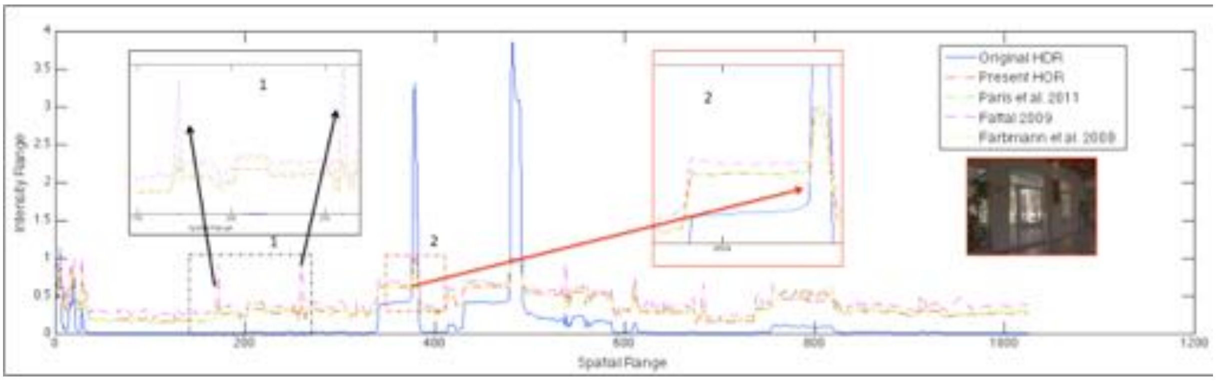

Figure 2: Intensity profile for the tone mapping operators on an HDR mage for line 300: The 1st zoomed area, clearly shows how Fattal's [11] method (undesirably) increases the intensity profile to the maximum value of 1. In the 2nd zoomed area (Paris et al. [9] green line), the intensity profile is modified.

dent metric (DRIM) introduced by Aydin et al. [12] for [10, 11, 9] and the technique proposed in this paper. The original HDR image is used as reference, and the output of the tone mapping operator is compared to it. A certain amount of lost of contrast (green) is clearly visible, and this may change the overall image structure [12]. The map shows that using the present HOR reduces the number of pixels affected by loss of contrast by more than 50%.

Moreover, the intensity profile may change as shown in Figure 2. The Fattal method [11] may have an undesirable increase of the intensity profile to the maximum output value 1 (1^{st} zoomed area). The structure of the original profile may be undesirably modified (green line) as shown for the method [9] (2^{nd} enlarged area). These methods may result in prohibitive computational costs (see Paris et al. [9]). An efficient implementation [14] of the method presented by Paris et al. [9] is also discussed in Section 6.

The proposed approach retains the same advantages introduced by the traditional edge aware approaches such as Paris et al. [9], and Fattal [11], namely with respect to obtaining local properties and providing robust smoothing, hence avoiding the use of pixels from both sides of the edge. The main contributions of this work can be summarized as follows:

1. Establish a link between the robust smoothing concept to the reconstruction problem of a non-smoothed function.
2. Achieve a complex solution of the edge-aware problem, through a simple and flexible point-wise manipulation by using HOR method.
3. Propose an edge-aware filter that produces halo free results; reduces the changes in the image structure as defined by the DRIM metric and its computational cost is increasing linearly with respect to the number of the input pixels N.

2. Related Work

Edge Aware Filters

Edge aware techniques are used to smooth an image while keeping its edges intact, preventing pixels located on one side of a strong edge from influencing pixels on the other side. This concept can be used to separate high frequency information from low frequency information such as texture and details. Once this separation is peformed the high and low frequencies information can be independently manipulated and re-composed.

In the past, techniques able to preserve edges [6, 8, 5] have been applied to image manipulation [15, 16, 17, 11]. These techniques produce acceptable results, but often introduce visible ringing effects arising from the Poisson equation [15] and filtering, as discussed in [10, 8]. Moreover, they need several parameters, that are image dependent, making their set-up difficult for practical applications [17]. Our approach offers a solution, that produces results at least as good as the above techniques, runs linearly in time with respect to the number of the input pixels and is not dependent on a large number of parameters.

Multi-Scale Edge Aware Filters

Recently, several edge-aware techniques that can be used in the multi-scale framework, have been presented. Typically, these methods exploit the multi-scale approach by making use of pyramid mechanisms such as Laplacian [18], Gaussian [19], and Wavelets [20].

The Laplacian approach, in the context of edge-aware, has been recently revised by Paris et al. [9] through the use of local transformation which makes the Laplacian approach suitable for edge-aware operations. Farbman et al. [10] employed the weighted least square to build an alternative edge preserving operator and extend it to multi-scales as well. Fattal et al. [15] used the Gaussian Pyramid to compress the high dynamic range of the input image, followed by the full image reconstruction through the use of the Poisson solver.

The aforementioned techniques share with our approach the multi-scale 'philosophy', but are using different methods such as the Laplacian [10, 9] and Gaussian [15] pyramids. Moreover, they are based on the solution of a linear system [10], a Poisson solver [15], or bilateral filtering all of which generate artifacts around edges [8]. Li et al. [21] proposed a multi-scale approach based on wavelets where each sub-band signal is modified using a gain map that controls the local contrast. Fattal [11] presented an edge avoiding technique based on a second generation wavelet. Our approach integrates within the wavelet mechanism a HOR technique that does not require any edge-stop function for computing a large set of weights in the interpolation step as in [11]. Consequently, using the present approach there is no need for any particular precaution against the strong edges and distortions of the image structure are reduced.

3. Background

Fixed stencil approximation techniques, such as piecewise linear and cubic interpolation, are often used to reconstruct the missing points of a function. These methods are working well in the case where the function is smooth; however, if the function is only piece-

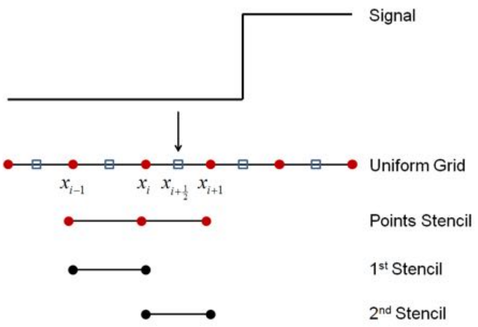

Figure 3: Example of the HOR scheme mechanism. (Top row) The original staircase signal. (2^{nd} row) The uniform grid points: (circle red) input points, (square blue) points to be interpolated. (3^{rd} row) The stencil points used by the HOR scheme. (4^{th} and 5^{th} rows): Two separated stencils used to define the two interpolants by the HOR scheme.

wise smooth the fixed stencil approximation may not be adequate near discontinuities. In fact, oscillations at the function discontinuities are visible,

Essential Non-oscillatory Scheme

Essential Non-oscillatory Schemes (ENO) have been introduced by Harten et al. [1] to solve this problem. The ENO scheme makes use of adaptive stencils, thus the use of discontinuity cells is avoided. Let us consider a signal function $f(x)$ with given grid of points of evaluated values such as $v[i] = f[x_i]$.

The ENO scheme reconstructs f from the point values v assuming that f is piecewise polynomial. This means that for each cell $I_i \equiv [x_{i-1}, x_{i+1}]$ a polynomial interpolant $p_i(x)$ is defined using the set of points defined in the stencil S_i. The idea is to find a stencil of $k+1$ consecutive points, including x_{i-1} and x_{i+1}, where the signal $f(x)$ is the smoothest in this stencil when comparing it with the other possible stencils. To evaluate the smoothness of $f(x)$ we can use the Newton divide differences of f:

$$\begin{array}{c} f[x_0] \equiv f(x_0); \\ f[x_0, x_1] \equiv \frac{f[x_0]}{(x_0-x_1)} + \frac{f[x_1]}{(x_1-x_0)}; \\ .... \end{array} \quad (1)$$

In general, the *j-th* degree divided difference of $f(x)$ is equivalent to

$$f[x_{i-1}, .., x_{i+j-1}] \equiv \frac{f[x_i, .., x_{i+j-1}] - f[x_{i-1}, .., x_{i+j-2}]}{x_{i+j-1} - x_{i-1}}. \quad (2)$$

Starting from a two points stencil

$$S_2(i) = x_{i-1}, x_{i+1}, \quad (3)$$

the linear interpolation of the stencil S_2 in a Newton form is

$$p_1(x) = f[x_{i-1}] + f[x_{i-1}, x_{i+1}](x - x_{i-1}). \quad (4)$$

To expand the stencil we have two possibilities, either add the left neighbor x_{i-2} or the right one x_{i+2}. In both cases this will be a quadratic interpolation polynomial. This will differ from the linear polynomial of eq. 4, by the same function multiplied by two different constants. These constants are the two 2-*nd* degrees of divided differences of $f(x)$ in two different stencils defined by the left and right neighbors.This procedure is continued until the $k+1$ points in the stencil are reached.

High Order Interpolation Scheme (HOR)

The typical problem of the ENO scheme is that it can exhibit oscillatory behavior and is also fairly expensive in its implementation [22]. As an alternative, the weighted ENO (WENO) variant has been proposed[1]. WENO uses a convex combination of all the corresponding interpolating polynomials on the stencil to compute an approximated polynomial for each cell (Figure 3). A convex combination is a linear combination where the coefficients (weights) are all positive and their sum is equal to 1. The key points of the reconstruction scheme are (at 3^{rd} order accuracy):

1. Stencils definition: Taking a cell defined in the interval $[x_{i-1/2}, x_{i+1/2}]$ (see Figure 3), the stencils are defined as [22]

$$\begin{array}{l} S_1 = (x_{i-3/2}, x_{i-1/2}, x_{i+1/2}); \\ S_2 = (x_{i-1/2}, x_{i+1/2}, x_{i+3/2}) \end{array} \quad (5)$$

2. Interpolation polynomials: For each stencil the linear interpolation polynomial is computed as

$$\begin{array}{l} p_1 = f[x_i] + \frac{f[x_i]-f[x_{i-1}]}{\Delta_x}(x - x_i); \\ p_2 = f[x_i] + \frac{f[x_{i+1}]-f[x_i]}{\Delta_x}(x - x_i) \end{array} \quad (6)$$

where the $f[x]$ elements are the available data points of the function to be reconstructed (red points in Figure 3).

3. Convex combination: The interpolation polynomials are combined following a convex combination

$$P_i = \frac{a_0^i}{a_0^i + a_1^i} p_1 + \frac{a_1^i}{a_0^i + a_1^i} p_2 \quad (7)$$

where

$$\begin{array}{l} a_0^i = \frac{C_0^i}{(\epsilon+(IS)_1)^{2.0}}; \\ a_1^i = \frac{C_1^i}{(\epsilon+(IS)_2)^{2.0}} \end{array} \quad (8)$$

[1] WENO schemes have been widely used in computational fluid dynamics; see, for example, Drikakis et al. [23] [24] [25] and references therein

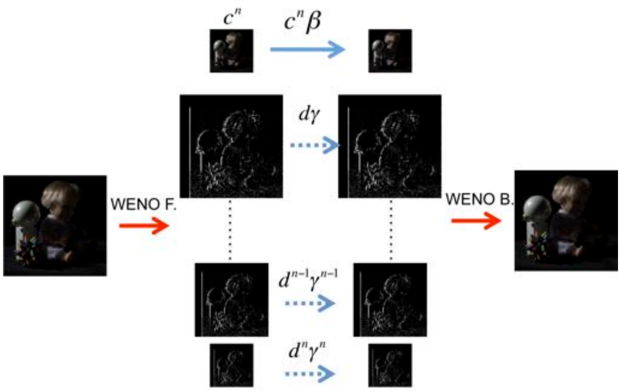

Figure 4: Overview of the present approach. Firstly, a pyramid representation of the input HDR image is produced using a forward wavelet lifting scheme with integrated the HOR interpolation method presented in this paper. Secondly, the coarse level of the pyramid structure (blue continue arrow) and the details levels (blue dashed arrows) are manipulated. Thirdly, the modified pyramid is collapsed to reconstruct the output tone mapped image. This is done, using the backward wavelet lifting scheme with integrated the HOR interpolation model.

IS are the smoothness indicators, which are calculated as $(IS)_1 = (f[x_i] - f[x_{i-1}])^{2.0}$ and $(IS)_2 = (f[x_{i+1}] - f[x_i])^{2.0}$. The gradient magnitude is well known to be a good estimator of edge information. Based on this observation, we have used the image gradient to select the coefficients C as given by [22], allowing the interpolation step to be aware of edge information in order to avoid an edge-stopping function.

- $\partial E(f)/\partial f > 0$: $C_0^i = 1/2$ and $C_1^i = 1$;
- $\partial E(f)/\partial f < 0$: $C_0^i = 1$ and $C_1^i = 1/2$.

4. HOR Wavelet Scheme

In this paper we propose a robust smoothing through the use of a polynomial interpolant that makes use of the smoothest stencils. It is integrated in a wavelet scheme (lifting scheme) to take advantage of the multi-scale representation such as the capability to retain image information at different scale. Figure 4 shows the principle of the present approach. Firstly, a pyramid representation of the original input image I is produced using a forward wavelet lifting WENO scheme. Secondly, the coarse (blue continued arrows) and fine levels (blue dashed arrow) are manipulated. Thirdly, the modified multiscale representation is collapsed to the output image using the backwards wavelet lifting WENO scheme. A multi-scale representation can be obtained by making use of a nested series of decimation D and reconstruction R operators. As a D operator, we have used a simple

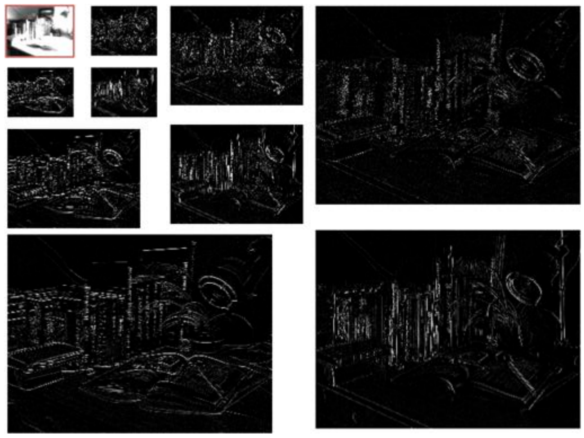

Figure 5: Pyramid image representation, after having applied the forward wavelet lifting WENO scheme. The coarse level is the image at the upper left corner (with red frame). The other images are representing the details, at different levels, for the horizontal, diagonal and vertical directions.

splitting operation which separates the pixels of the input at level k in two different grids based on the index number (odd and even). For the R operator the WENO scheme has been employed according to which the level k is reconstructed from $k+1$ using eq. 9:

$$\begin{gathered}\tilde{I}^k[x,y] = w_0[x,y](I^{k+1}[x-1,y]+ \\ \frac{I^{k+1}[x-1,y]-I^{k+1}[x-3,y]}{[x-1,y]-[x-3,y]}([x,y]-[x-1,y])) \\ +w_1[x,y](I^{k+1}[x-1,y]+ \\ \frac{I^{k+1}[x+1,y]-I^{k+1}[x-1,y]}{[x+1,y]-[x-1,y]}([x,y]-[x+1,y])).\end{gathered} \tag{9}$$

Eq. 9 is equivalent to eq. 7 where w_0 and w_1 are its factorial terms.The difference in the indices between eq. 9 and eq. 7 is due to the fact that we have inserted zero pixels at $k+1$ level and would like to retain integer numbers in the indexing of the grid. Fattal [11] presented a robust average operator, for both type of wavelet approaches, *red − black* and *weighted CDF*, making use of an edge stop function to compute the prediction weights. In our case, as described in *eq.* 7, we present a convex combination of polynomial interpolants. However, these polynomial interpolants are linear, thus we can consider the overall operator as a combination of linear interpolants.

At the boundaries of the input image, we have adopted a standard extrapolation approach to generate the missing values in the stencil . The restored $\tilde{I}^k$ level is later used to obtain the details of the $k+1$ level $d^{k+1} = I^k - \tilde{I}^k$. To preserve the overall sum of the coarse elements I_{k+1}, and based on the fact that the operator R can be seen as combination of two linear interpolants we have decided to use a linear interpolator as update-operator U:

$$U(d^{k+1})[x, y] = \frac{d^{k+1}[x-1, y] + d^{k+1}[x+1, y]}{4}; \quad (10)$$

and the level $k+1$ of coarse elements is updated using $I^{k+1} = I^{k+1} + U(d^{k+1})$.

This process is repeated both for the rows and columns of the input image.

Discussion An example of the behaviour of the present HOR, integrated in the wavelet scheme, is shown in Figure 5. The coarse, c, and 'details' coefficients, d, (vertical, diagonal and horizontal) for three levels are shown. Edges are detected by the wavelet scheme avoiding the influence of pixels on both sides at each scale. This is obtained without the introduction of an edge stop function utilized for the computation of the set of weights used in the interpolation step as proposed by Fattal [11] .

5. Tone Mapping Manipulation

In this subsection, we will show how to make use of the proposed technique in the classical tone manipulation problem. Tone manipulation allows to reduce the intensity of the luminance range of HDR content. This objective is achieved through compression of large-scale variation and keeping the fine level information. The filtering approach is applied to the natural logarithmic scale of the luminance, keeping the color ratio unaltered as in Paris et al. [9], using a gamma correction of 2.2.

To manipulate the tone and the details of the input HDR image, we have followed a similar approach to the one used by Fattal [11]. The tone is linearly manipulated modifying the coarse coefficient c of the coarsest level n through a parameter β, as βc^n. This allows us to achieve the compression of the vast dynamic range available in the input HDR image. A second parameter γ is used to manipulate the details. This is obtained from the progressive decreasing of the 'details' coefficients d^k, such as $\gamma^k d^k$ where k is the number of levels varying between 1 to n. The β and γ parameters are in the range of (0.0, 1.0].

Since our approach shares several aspects with the technique presented by Fattal [11], we first provide an analysis and comparison to show how the present technique performs with respect to the preservation of edges, while at the same time adjusting the tone of the input image.

Figure 6: Comparisons with state-of-the-art method Fattal's method [11] . 1^{st} row: Fattal [11] using wavelet Red and Black model with $\alpha = 0.8$, $\beta = 0.11$ and $\gamma = 0.68$ - 2^{nd} row: the present approach with $\beta = 0.3$ and $\gamma = 0.7$ -2^{nd} column: Gradient of a zoomed area, it showing the degree of edge preservation.

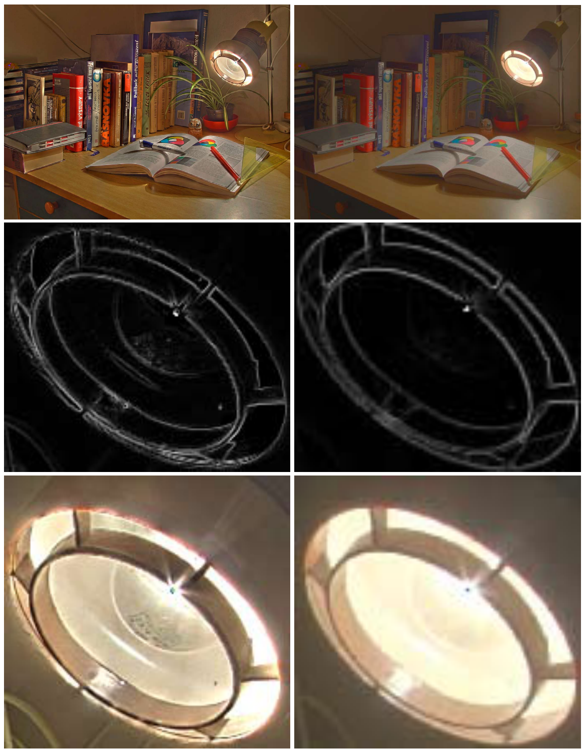

Figure 7: Comparisons of different methods. 1^{st} column: Fattal [11] using wavelet Red and Black model with parameters as per web project page [26] - 2^{nd} column: The present approach with $\beta = 0.7$ and $\gamma = 0.9$ - 2^{nd} row: Gradient of the zoomed area in the 3^{rd} row. Distortions at the edges are visible.

(a) Fattal [11] $\beta = 0.7$ - Weak (b) Fattal [11] $\beta = 0.5$ - Strong

Figure 8: Results from the application of Fattal's et al. [11] technique making use of the new contractive concave mapping as specified in [26].

The present technique produces results comparable to this state-of-the-art operator, while offering the advantage of not using an extra edge-stop function. The technique of [11] is capable to capture more details but at the cost of introducing some distortions at the edge level, as shown in Figures 7 (a) (zoomed lamp area and its edge map) and 6 (b) (edge map).

One may reduce these distortions by making use of a new compression technique, as suggested in [26] (Figure 8). However, artifacts may appear as shown in Figure 8 (b) 2^{nd} row.

6. Experimental Results

The HOR approach has been implemented in Matlab and the experiments have been performed on a Mackbook air with Intel i7-core CPU 1.8 GHz, 64-bit machine and 4GB of RAM. We have compared our technique with the latest edge aware state-of-the-art multi-scale approaches, applied to the tone mapping problem, such as[11, 9, 10]. We have used the Matlab code as well as parameters provided by the authors.

We have chosen the set of images shown in Figure 9. This set consists of 18 images with different dynamic range that span from outdoor to indoor and from light to dark illumination conditions.

Figure 9: Images used in the experiments. The numbering in Tables 1 and 2 follows the order of the images from the top to the bottom and from the left to the right.

6.1. Quality

To provide a fair comparison, we have selected the parameters of the different techniques to convey similar appearance in term of contrast, edges and details preservation to all the techniques presented in this comparison.

We may observe that the DRIM metric is measuring changes in contrast, in other words the overall appearance of the image, and it is not able to detect if small-scale details are not well preserved. On the other hand, edge-aware techniques are able to preserve well small-scale details. This is preserved intrinsically by the mechanisms described in the previous sections as well as by the results shown here that are comparable with the existing state-of-the-art edge aware technique [11].

Based on the fact that small-scale details are to certain extent well reproduced by the edge-aware techniques, our objective was to examine how these techniques are able to convey the overall appearance of the input HDR into the tone mapped result. In doing so, we have decided to use the DRIM metric as specified below.

Since the DRIM metric accepts cd/m^2 values, the input images need to be calibrated. In the case of the tone mapped input image, we need to linearize the input signal and then map it to the dynamic range of the display where the image will be visualized. In our case, the γ value used for the linearization step is 2.2, and the dynamic range chosen is [0.5, 100] cd/m^2 . In the case of the HDR input image, there was no need to linearize the signal, and the dynamic range has been chosen as [0.015, 3000] cd/m^2.

DRIM Results Discussion

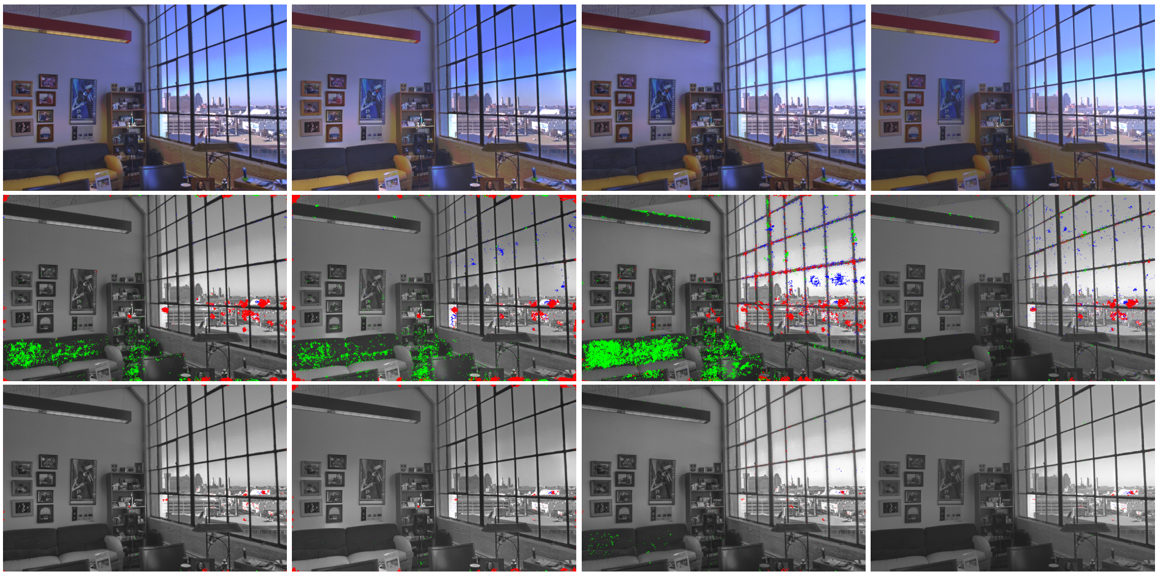

Figure 10: Output and DRIM comparison with state-of-the-art edge aware approaches.1^{st} - row output of the edge aware technique; 2^{nd} row - DRIM metric [12] with probability of 75%; 3^{rd} row - DRIM metric [12] with probability of 95%. Parameters used - Farbmann et al. [10] multiscale approach balanced - Fattal's [11] $\alpha = 0.9, \beta = 0.19$ and $\gamma = 0.5$ - Paris et al. [9] $\sigma_r = log(2.5)$, $\alpha = 0.5$ and $\beta = 0.0$ (for conveying the local effect) - The Present HOR $\beta = 0.7, \gamma = 0.9$.

Tables 1 and 2 show the results of the DRIM metric applied to the test set images. The numbers represent the percentage of pixels with probability for the distortion to be perceived by the HVS. Tables 1 and 2 show the results with probability 95% and 75%, respectively. The colors used to depict the type of distortion are the same with those used to describe the distortion - *R* (red) reversal, - *G* (green) lost and - *B* (blue) amplification of contrast. We have colored the methods that show the higher probability, as well as the ones that show significant percentage of pixels with the specified probability. In the case of probability 95%, the significant distortion introduced by the state-of-the-art edge aware methods, as well as by the present HOR is mostly due to the loss of contrast; neither reversal nor amplification of contrast are significant. The lost of contrast is attributed to the fact that the edge-aware methods are using simple linear scaling for compressing the large luminance dynamic range. This may affect the overall preservation of local contrast. With probability 95% the state-of-the-art methods may present high percentage of pixels affected by loss of contrast. This is the case of the images 1, 3, 5, 11,13 and 14. In most of the other cases, this number is negligible. For the images 1, 13 and 14, the HOR shows a slightly higher percentage value for the loss of contrast. However, this value is either comparable or lower than the value provided by the state-of-the-art edge-aware methods.We have also tried to analyze the results of the DRIM metric at lower probability such as 75% and the results are shown in Table 2. As expected, the percentage of pixels is drastically increased and more images are affected by a significant percentage value. In this case, reversal of contrast (red) and in some cases amplification of contrast (blue) may appear. In the case of loss of contrast the Fattal [11] and Paris et al. [9] results show that the majority of the images are affected by this type of distortion. This type of distortion also affects the present HOR, but when compared with the state-of-the-art edge-aware methods shows a lower percentage of pixels affected by this distortion.

Only in the case of image 18 the present HOR shows higher value for the loss of contrast. However, this percentage value is quite small and it is not actually perceivable by the HVS. The results are also affected by the reversal of contrast. In particular, several results of Fattals [11] method are showing this distortion. The present HOR shows reversal of contrast higher than the other methods only for three images (11, 12 and 18). Finally, the amplification of contrast (blue) does almost not exist, and the only image that is affected by using the proposed HOR is the image 15.

DRIM Visual Analysis

Figures 10, 11, 13 and 14 show results with the corresponding DRIM distortion maps. Figure 10 and Figure 11 compares the DRIM maps at probability 75% (2^{nd} row) and at 95% (3^{rd} row) for each output result.

Figure 11: Output and DRIM comparison with state-of-the-art edge aware approaches.1^{st} - row output of the edge aware technique; 2^{nd} row - DRIM metric [12] with probability of 75%; 3^{rd} row - DRIM metric [12] with probability of 95% (for both images). Parameters used - Farbmann et al. [10] multiscale approach balanced - Fattal's [11] $\alpha = 0.8$, $\beta = 0.12$ and $\gamma = 0.9$ - Paris et al. [9] $\sigma_r = log(2.5)$, $\alpha = 0.5$ and $\beta = 0.0$ (for conveying the local effect) - The Present HOR $\beta = 0.7$, $\gamma = 0.9$.

Image	Farbman [10]	Fattal [11].	Paris [9]	HOR
1 AhwahneeGL	R 0.28 G 3.72 B 0.0	R 0.22 G 3.0 B 0.0	R 0.6 G 6.16 B 0.0	R 0.26 G 5.24 B 0.0
2 Belgium	R 0.0 G 0.0 B 0.0	R 0.11 G 0.35 B 0.0	R 0.0 G 0.0 B 0.0	R 0.0 G 0.0 B 0.0
3 Cadik1	R 0.0 G 1.34 B 0.0	R 0.2 G 5.1 B 0.73	R 0.0 G 3.44 B 0.0	R 0.0 G 0.0 B 0.0
4 smallOffice	R 0.0 G 0.0 B 0.0	R 0.14 G 0.0 B 0.0	R 0.0 G 0.0 B 0.0	R 0.0 G 0.0 B 0.0
5 Cadik2	R 0.0 G 4.0 B 0.0	R 0.0 G 3.02 B 0.0	R 0.0 G 8.4 B 0.0	R 0.0 G 0.89 B 0.0
6 Kitchen	R 0.0 G 0.0 B 0.0	R 0.19 G 0.22 B 0.0	R 0.0 G 0.8 B 0.0	R 0.0 G 0.0 B 0.0
7 GroveD	R 0.0 G 0.0 B 0.0	R 0.29 G 0.0 B 0.0	R 0.0 G 0.0 B 0.0	R 0.0 G 0.0 B 0.0
8 Synagouge	R 0.0 G 0.0 B 0.0	R 0.13 G 0.0 B 0.0	R 0.0 G 0.0 B 0.0	R 0.0 G 0.0 B 0.0
9 Cathedral	R 0.0 G 0.0 B 0.0	R 0.23 G 0.0 B 0.0	R 0.0 G 0.0 B 0.0	R 0.17 G 0.0 B 0.0
10 Clockbui	R 0.0 G 0.0 B 0.0	R 0.14 G 0.0 B 0.0	R 0.0 G 0.0 B 0.0	R 0.0 G 0.0 B 0.0
11 Desk	R 0.0 G 0.86 B 0.0	R 0.31 G 3.0 B 0.0	R 0.11 G 1.78 B 0.0	R 0.23 G 0.96 B 0.0
12 FogMap	R 0.13 G 0.8 B 0.0	R 0.14 G 0.79 B 0.0	R 0.0 G 0.0 B 0.0	R 0.25 G 0.74 B 0.0
13 Memorial	R 0.1 G 2.4 B 0.0	R 0.27 G 7.1 B 0.0	R 0.24 G 7.9 B 0.0	R 0.13 G 3.9 B 0.0
14 DesignCenter	R 0.0 G 4.35 B 0.0	R 0.6 G 20.6 B 0.0	R 0.0 G 18.0 B 0.0	R 0.18 G 4.2 B 0.0
15 Tinterna	R 0.0 G 0.0 B 0.0	R 0.27 G 0.0 B 0.0	R 0.0 G 0.0 B 0.0	R 0.0 G 0.0 B 0.0
16 Yosemite	R 0.0 G 0.0 B 0.0	R 0.32 G 0.0 B 0.0	R 0.0 G 0.0 B 0.0	R 0.0 G 0.0 B 0.0
17 Doll	R 0.0 G 0.0 B 0.0	R 0.0 G 0.0 B 0.0	R 0.0 G 0.0 B 0.0	R 0.31 G 0.13 B 0.0
18 Paull	R 0.0 G 0.0 B 0.0	R 0.0 G 0.0 B 0.0	R 0.0 G 0.0 B 0.0	R 0.11 G 0.0 B 0.0
AVERAGE	**R 0.028 G 0.97 B 0.0**	**R 0.19 G 2.38 B 0.041**	**R 0.053 G 2.2 B 0.0**	**R 0.09 G 0.89 B 0.0**

Table 1: DRIM results over the set of images presented in Figure 9. We show the percentage of pixels with probability of 95% that present the distortion of reverse (*R*), loss (*G*), or amplification (*B*) of contrast.

The visual analysis of the results shows that in the case of probability 75% the state-of-the-art methods show a consistent number of distorted pixels localized in large areas, when compared with the present HOR. On the other hand, when the probability increases to 95%, the size of these areas are either reduced or are almost not affected by any distortion. However, in some cases the state-of-the-art methods are still showing large areas of lost of contrast (green) and reversal of contrast (red).

Figures 13 and 14 are showing other results with the distortion maps with probability at 95%, where the all methods are showing similar behavior..

Comparison with Simpler TMO's

One can observe that the global operators are faster and convey an overall better appearance (Artusi et al. [28]). For this purpose, we have computed the DRIM maps for a well known global version of two TMOs published by by Reinhard et al. [27] and Drago et al. [27]. The comparison is limited to the global operator showing that the quality of the results is not comparable with the state-of-the-art edge aware techniques.

The results are shown in Figure 12 for the distortion maps at probability of 95%.

The results reveal that the DRIM obtained for the Reinhard et al. [27] and the Drago et al. [27] operators often show larger areas of amplification of contrast; see the window area in Figure 12, in comparison with the results obtained by the majority of the edge-aware techniques employed in this experiment.

Figure 12 ($2^n d$ row shows reversal of contrast, in large areas of the window, for both global operators. On the other hand, the edge-aware techniques have very tiny areas affected by reversal of contrast. Moreover, we emphasize in general that global operators are not designed for edge-awareness and do not encapsulate mechanisms for retaining the fine details at different spatial scale, as in the case of the present HOR and edge-aware techniques.

6.2. *Computational Analysis*

Another aspect that needs to be taken into account is the computational cost associated with the different algorithms. Here, we have performed a computational cost analysis for the proposed technique versus other state-of-the-art techniques.

Our approach presents computational complexity and associated cost comparable to the one presented in [11, 10] and outperforming the method of [9] .

Specifically, the method presented by Paris et al. [9] requires 1738 sec to process an image size of 800x525, 420 sec for an image size of 400x262 and 190 sec. for an image size of 267x174. When compared with the computational cost of our method and the approaches of [11, 10], the computational cost is significantly reduced: 14 sec to process an image size of 800x525, 3 sec for an image size of 400x262, and 1 sec for an image size of 267x174.

Image	Farbman [10]	Fattal [11].	Paris [9]	HOR
1 AhwahneeGL	R 1.0 G 15.0 B 0.17	R 0.91 G 12.6 B 0.15	R 1.96 G 21 B 0.2	R 1.33 G 18.5 B 0.11
2 Belgium	R 0.13 G 0.0 B 0.0	R 0.9 G 2.73 B 0.0	R 0.27 G 0.18 B 0.15	R 0.14 G 0.0 B 0.4
3 Cadik1	R 0.4 G 9.2 B 0.0	R 1.1 G 16.6 B 0.0	R 0.31 G 17.4 B 0.12	R 0.13 G 1.72 B 0.14
4 smallOffice	R 0.43 G 0.58 B 0.0	R 0.57 G 0.67 B 1.63	R 0.78 G 1.77 B 0.45	R 0.24 G 0.0 B 0.24
5 Cadik2	R 0.4 G 16.7 B 0.0	R 0.44 G 12.8 B 0.0	R 0.45 G 25 B 0.18	R 0.12 G 6.7 B 0.0
6 Kitchen	R 0.0 G 0.0 B 0.0	R 0.92 G 4.9 B 0.0	R 0.3 G 0.11 B 0.16	R 0.0 G 0.59 B 0.0
7 GroveD	R 0.15 G 0.0 B 0.13	R 5.9 G 0.42 B 0.67	R 0.5 G 0.0 B 0.32	R 0.79 G 0.0 B 0.4
8 Synagouge	R 0.18 G 0.1 B 0.15	R 2.4 G 3.8 B 0.1	R 0.1 G 0.0 B 0.3	R 0.3 G 0.38 B 0.81
9 Cathedral	R 0.0 G 0.0 B 0.15	R 2.29 G 1.14 B 0.57	R 0.64 G 0.0 B 0.0	R 1.66 G 0.76 B 2.0
10 Clockbui	R 0.29 G 0.0 B 0.0	R 0.61 G 0.0 B 0.20	R 1.12 G 0.0 B 0.6	R 0.6 G 0.18 B 0.24
11 Desk	R 0.4 G 3.9 B 0.12	R 2.28 G 10.2 B 0.18	R 1.9 G 8.6 B 0.54	R 3.03 G 5.11 B 0.73
12 FogMap	R 0.34 G 0.73 B 0.0	R 0.0 G 2.15 B 0.03	R 1.1 G 19 B 0.0	R2.45 G 18.6 B 0.0
13 Memorial	R 0.6 G 14.8 B 0.0	R 1.55 G 23.5 B 0.0	R 1.9 G 26.9 B 0.0	R 0.97 G 18.7 B 0.0
14 DesignCenter	R 0.31 G21.7 B 0.0	R 3.8 G 30.5 B 0.0	R 0.55 G28.7 B 0.0	R 1.35 G 22.0 B 0.0
15 Tinterna	R 0.5 G 0.0 B 0.6	R 3.7 G 0.63 B 0.55	R 0.18 G 0.11 B 0.57	R 0.17 G 0.0 B 4.36
16 Yosemite	R 0.23 G 0.0 B 0.0	R 4.1 G 0.49 B 0.21	R 0.38 G 0.0 B 0.48	R 0.15 G 0.0 B 0.45
17 Doll	R 0.13 G 0.0 B 0.35	R 0.82 G 3.6 B 0.14	R 0.35 G 0.31 B 0.2	R 1.7 G 1.5 B 0.53
18 Paull	R 0.18 G 0.0 B 0.1	R 1.8 G 0.36 B 0.25	R 0.24 G 0.1 B 0.4	R 2.5 G 1.22 B 0.4
AVERAGE	**R 0.32 G 4.81 B 0.098**	**R 1.89 G 7.06 B 0.26**	**R 0.72 G 8.29 B 0.26**	**R 0.98 G 5.33 B 0.59**

Table 2: DRIM results over the set of images presented in Figure 9. We show the percentage of pixels with probability of 75% that present the distortion of reverse (*R*), loss (*G*), or amplification (*B*) of contrast.

Recently, Aubry et al. [14] presented a fast implementation of Paris et al. [9] technique that significantly improves its computational performances (50 times faster). However, our comparison is done on the Matlab implementation of the all techniques used in the evaluation, as provided by the authors, without including any optimization. Even if we apply the 50-fold improvement in the measured time of the Matlab implementation of Paris et al. [9], the present HOR delivers an excellent overall performance.

7. Concluding remarks

We have introduced a new edge preserving technique that makes use of a HOR method, which is able to preserve edges without introducing artifacts and reducing any changes in the image structure when compared to the state-of-the-art edge preserving operators. The present method does not require an extra stop-edge function, thus offering simplicity. Futhermore, its computational cost increases linearly in time. We have demonstrated the accuracy of the present technique on a variety of images and parameter settings. The use of the HOR technique in other applications such as details enhancement and image colorisation is also possible and will be part of future work. The proposed HOR technique will be further implemented in graphics hardware with reference to video applications, allowing substantial improvements in computational performance.

8. Acknowledgments

This work was partially supported by Ministry of Science and Innovation Subprogramme Ramon y Cajal RYC-2011-09372, TIN2013-47276-C6-1-R from Spanish government, 2014 SGR 1232 from Catalan government, NSFC-Guangdong Joint Fund (U1135003, Natural Science Foundation of China (NSFC) (No. 61320106008).

References

[1] A. Harten, B. Engquist, S. Osher, S. Chakravarthy, Uniformly high order essentially non-oscillatory schemes, Journal of Computational Physics 1987.

[2] C. W. Shu, Essentially non-oscillatory and weighted essentially non-oscillatory schemes for hyperbolic conservation laws, Tech. rep., ICASE Report No. 97-65, NASA - CR-97-206253 (1997).

[3] T. F. Chan, H. M. Zhou, Eno-wavelet transforms for piecewise smooth functions, SIAM Journal on Numerical Analysis 40 (2002) 1369–1404.

[4] H. Boucenna, M. Halimi, Image segmentation by the level set methods using third order weno, 5th International Conference: Sciences of Electronic, Technologies of Information and Telecommunications 2009.

[5] P. Perona, J. Malik, Scale-space and edge detection using anisotropic diffusion, IEEE Transactions on Pattern Analysis and Machine Intelligence 12 (1990) 629–639.

[6] C. Tomasi, R. Manduchi, Bilateral filtering for gray and color images, Proceedings of the IEEE International Conference on Computer Vision (1998) 839–846.

[7] Z. Su, X. Luo, A. Alessandro, A novel image decomposition approach and its applications., The Visual Computer 29 (10) (2013) 1011–1023.

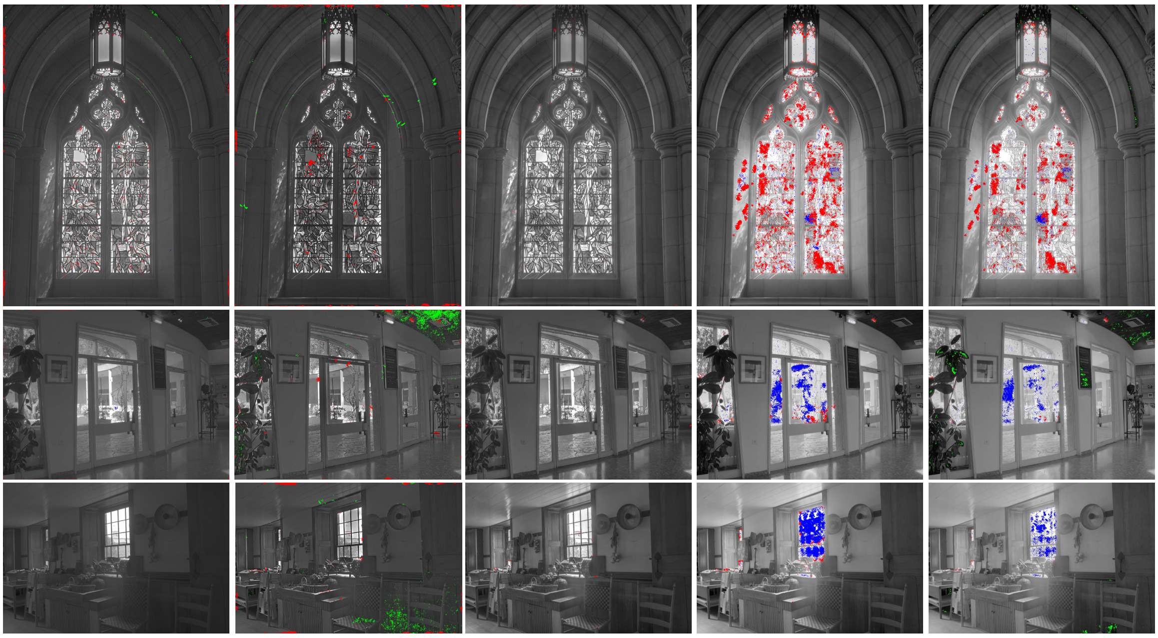

Figure 12: DRIM comparison with state-of-the-art edge aware approaches and simple TMO. DRIM metric [12] with probability of 95%. Farbman et al. [10] DRIM output is omitted because of the similarities in the results with the one obtained with the present HOR.

[8] B. C. A. Buades, J. M. Morel, The staricasing effect in neighborhood filters and its solution, IEEE Journal on Transactions on Image Processing 15 (2006) 1499–1505.

[9] P. Silvan, S. W. Hasinoff, J. Kautz, Local laplacian filters: Edge aware image processing with a laplacian pyramid, ACM Transactions on Graphics (Proceedings of ACM SIGGRAPH 2011).

[10] Z. Farbman, R. Fattal, D. Lischinski, R. Szeliski, Edge-preserving decompositions for multi-scale tone and detail manipulation, in: ACM SIGGRAPH 2008 Papers, SIGGRAPH '08, ACM, 2008, pp. 67:1–67:10.

[11] R. Fattal, Edge-avoiding wavelets and their applications, ACM Trans. Graph. 28 (3) (2009) 1–10.

[12] T. O. Aydin, R. Mantiuk, K. Myszkowski, H.-P. Seidel, Dynamic range independent image quality assessment, ACM Trans. Graph. 27 (3) (2008) 69:1–69:10.

[13] F. Banterle, A. Artusi, K. Debattista, A. Chalmers, Advanced High Dynamic Range Imaging: Theory and Practice, AK Peters (CRC Press), Natick, MA, USA, 2011.

[14] M. Aubry, S. Paris, S. Hasinoff, J. Kautz, F. Durand, Fast and robust pyramid-based image processing, Tech. rep. (2011).

[15] R. Fattal, D. Lischinski, M. Werman, Gradient domain high dynamic range compression, ACM Trans. Graph. 21 (3) (2002) 249–256.

[16] J. Chen, S. Paris, F. Durand, Real-time edge-aware image processing with the bilateral grid, ACM Transactions on Graphics (Proceedings of ACM SIGGRAPH 2007).

[17] J. Tumblin, G. Turk, Lcis: A boundary hierarchy for detail-preserving contrast reduction, ACM Transactions on Graphics (Proceedings of ACM SIGGRAPH 1999).

[18] P. J. Burt, Edward, E. H. Adelson, The laplacian pyramid as a compact image code, IEEE Transactions on Communications 31 (1983) 532–540.

[19] P. J. Burt, Fast filter transform for image processing, Computer Graphics and Image Processing 16 (1) (1981) 20 – 51.

[20] A. N. Akansu, P. R. Haddad, Multiresolution Signal Decomposition: Transforms, Subbands, and Wavelets, Academic Press, 1992 and 2000 (2nd Ed.).

[21] Y. Li, L. Sharan, E. H. Adelson, Compressing and companding high dynamic range images with subband architectures, ACM Trans. Graph. 24 (2005) 836–844.

[22] X. Liu, S. Osher, T. Chan, Weighted essentially non-oscillatory schemes, Journal of Computational Physics 115 (1994) 200–212.

[23] A. Mosedale, D. Drikakis, Assessment of very high-order of accuracy in les models, ASME Journal of Fluids Engineering 129 (2007) 1497–1503.

[24] B. Thornber, A. Mosedale, D. Drikakis, On the implicit large eddy simulations of homogeneous decaying turbulence, Journal of Computational Physics 226 (2007) 1902–1929.

[25] D. Drikakis, M. Hahn, A. Mosedale, T. B., Large eddy simulation using high resolution and high order methods, Philosophical Transactions Royal Society A 367 (2009) 2985–2997.

[26] R. Fattal[link].
URL `http://www.cs.huji.ac.il/ raananf/projects/eaw/`

[27] E. Reinhard, M. Stark, P. Shirley, J. Ferwerda, Photographic tone reproduction for digital images, ACM Trans. Graph. 21 (3) (2002) 267–276.

[28] A. Artusi, O. Akyz, Ahmet, B. Roch, D. Michael, Y. Chrysanthou, A. Chalmers, Selective local tone mapping, proceedings IEEE International Conference on Image Processing (ICIP) 2013.

Figure 13: Output and DRIM comparison with state-of-the-art edge aware approaches. 1^{st} and 3^{rd} - rows output of the edge aware techniques; 2^{nd} and 4^{th} rows - DRIM metric [12] with probability of 95%. Parameters used - Farbmann et al. [10] multiscale approach balanced - Fattal's [11] α = 0.8, β = 0.19 and γ = 0.9; - Paris et al. [9] $\sigma_r = log(2.5)$, α = 0.5 and β = 0.0 (for conveying the local effect) - The Present HOR 1^{st} row: β = 0.4, γ = 0.8; 3^{rd} row: β = 0.6, γ = 0.8.

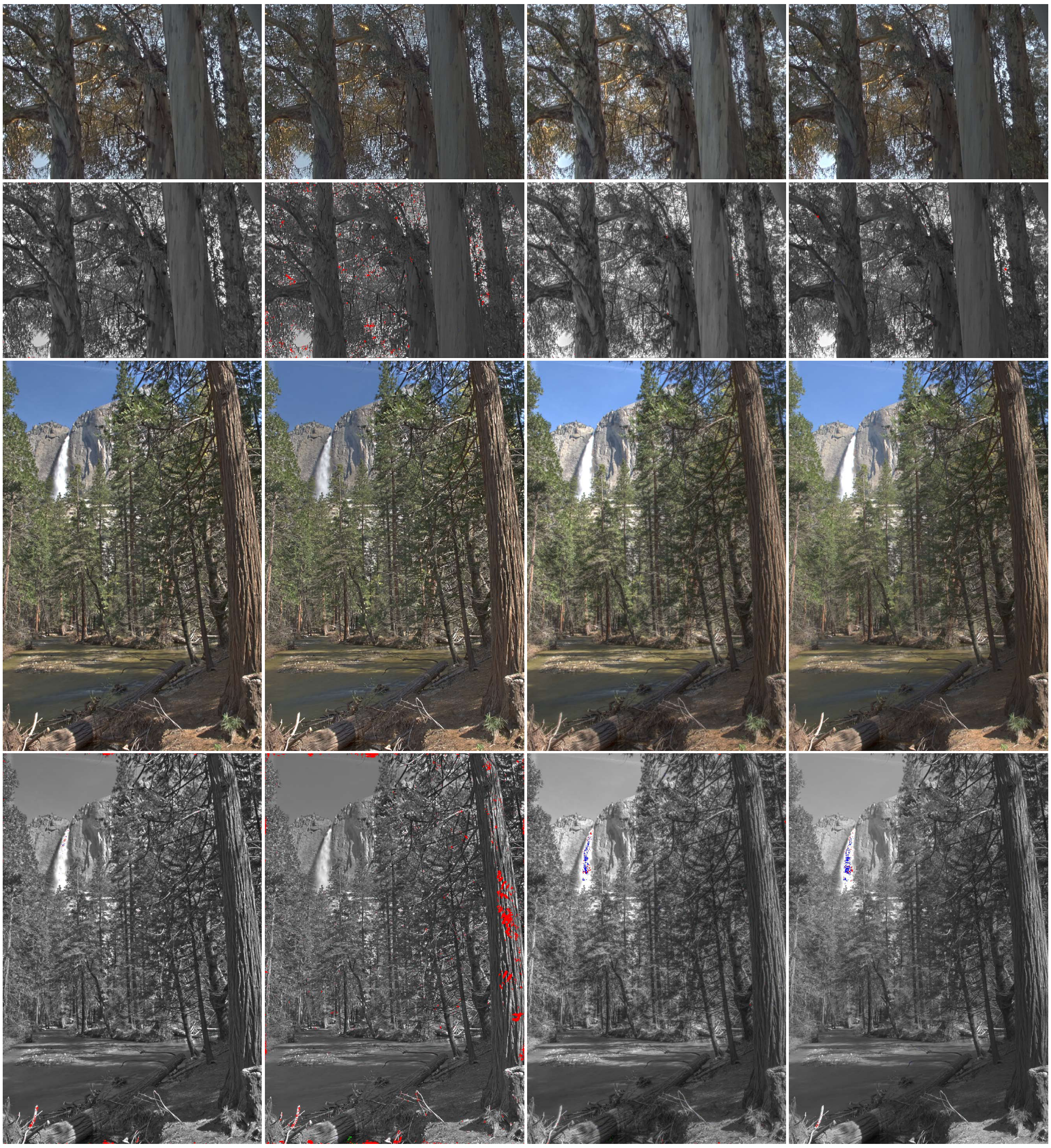

Figure 14: Output and DRIM comparison with state-of-the-art edge aware approaches. 1^{st} and 3^{rd} - rows output of the edge aware techniques; 2^{nd} and 4^{th} rows - DRIM metric [12] with probability of 95%. Parameters used - Farbmann et al. [10] multiscale approach balanced - Fattal's [11] α = 0.8, β = 0.19 and γ = 0.9; - Paris et al. [9] $\sigma_r = log(2.5)$, α = 0.5 and β = 0.0 (for conveying the local effect) - The Present HOR 1^{st} row: β = 0.6, γ = 0.9; 3^{rd} row: β = 0.7, γ = 0.9.